

Limits on the microlens mass function of Q2237+0305

J. S. B. Wyithe¹, R. L. Webster¹, E. L. Turner²

¹ School of Physics, University of Melbourne, Parkville, Vic, 3052, Australia

² Princeton University Observatory, Peyton Hall, Princeton, NJ 08544, USA

Email: swyithe@physics.unimelb.edu.au, rwebster@physics.unimelb.edu.au, elt@astro.princeton.edu

Accepted Received

ABSTRACT

Gravitational microlensing at cosmological distances is potentially a powerful tool for probing the mass functions of stars and compact objects in other galaxies. In the case of multiply-imaged quasars, microlensing data has been used to determine masses of the microlenses (eg. Lewis & Irwin 1996; Schmidt & Wambsganss 1998). However such measurements have relied on an assumed transverse velocity for the lensing galaxy. Since the measured mass scales with the square of the transverse velocity, published mass limits are quite uncertain. In the case of Q2237+0305 we have properly constrained this uncertainty in previous work by treating the transverse velocity as a variable, and shown that limits can be placed on its value (Wyithe, Webster & Turner 1999b). The distribution of light curve derivatives allows us to treat the relative rates of microlensing due to proper motions of microlenses, the orbital stream motion of microlenses and the bulk galactic transverse velocity quantitatively (Wyithe, Webster & Turner 1999a). By demanding that the microlensing rate due to the motions of microlenses in the bulge is the minimum that should be observed we determine lower limits of the average mass of stars and compact objects in the bulge of Q2237+0305. If microlenses in the bulge are assumed to move in an orbital stream the lower limit ranges between 0.005 and $0.023M_{\odot}$ where the systematic dependence is due to the fraction of smooth matter and the size of photometric error assumed. However, if the microlenses are assumed to move according to an isotropic velocity dispersion then a larger lower limit of 0.019 – $0.11M_{\odot}$ is obtained. A significant contribution of Jupiter mass compact objects to the mass distribution of the bulge is therefore unambiguously ruled out in this case.

Key words: gravitational lensing - microlensing - stellar masses.

1 INTRODUCTION

Q2237+0305 comprises a source quasar with a redshift of $z = 1.695$ that is gravitationally lensed by a foreground galaxy at $z = 0.0394$ producing 4 resolvable images with separations of $\sim 1''$. Each of the 4 images are observed through the galactic bulge which has an optical depth in stars that is of order unity (eg. Kent & Falco 1988; Schneider et al. 1988; Schmidt, Webster & Lewis 1998). In addition, the proximity of the lensing galaxy means that the effective transverse velocity may be high. The combination of these facts make Q2237+0305 the ideal object from which to study microlensing. Indeed, Q2237+0305 is the only object in which cosmological microlensing has been confirmed (Irwin et al. 1989; Corrigan et al. 1991). Numerical microlensing simulations (eg. Wambsganss, Paczynski & Schneider 1990) have shown that the statistics of microlensed high magnification events (HMEs) obtained from long term monitoring may

provide information on properties of the lens such as the stellar mass function and the percentage of mass in stars for the bulge. However, the monitoring period required is >100 years (Wambsganss, Paczynski & Schneider 1990). There are several other unknown quantities in the problem. These include the magnitude and direction of any transverse motion, as well as the source size. In particular, when the HME statistics of a given model are considered, the magnitude and direction of the transverse motion are degenerate with the density of caustics (a function of the mean compact object mass).

Microlensed fluctuation in the quasars continuum results from motion due to both a galactic transverse velocity and to the random proper motion or stream motion of stars and compact objects. Wyithe, Webster & Turner (1999a) define the equivalent transverse velocity as the transverse velocity in a model containing stars with static positions, that produces a rate of microlensing most closely resem-

bling that of a model containing stellar proper motions. Foltz et al. (1992) measured the central velocity dispersion of Q2237+0305 to be $\sim 215 \text{ km sec}^{-1}$, and theoretical models (Schmidt, Webster & Lewis 1998) predict a value of $\sim 165 \text{ km sec}^{-1}$. If the dispersion is isotropic then (as discussed in Wyithe et al. (1999b)) the equivalent transverse velocity calculated from the overall microlensing rate (all 4 images) of Q2237+0305 is larger than this value. The microlensing rate that results from the line-of-sight velocity dispersion (of an isotropic distribution) is therefore comparable to that of the likely transverse velocity. This means that the often made assumption that random proper motions provide a negligible contribution to microlensing in Q2237+0305 is incorrect.

While the microlensing rate that results from random stellar motions is dependent on the mean microlens mass, the equivalent transverse velocity (Wyithe, Webster & Turner 1999a,b) that describes the microlensing rate is not. We use this fact to break the degeneracy between microlensing rate and mean microlens mass, and hence to obtain useful limits on the mass function along the line-of-sight through the galactic bulge. These limits rely on results obtained for the effective transverse velocity from current monitoring data.

This paper is presented in 5 parts. Section 2 contains a general discussion of microlensing and the mass function. Section 3 discusses the numerical methods used to model microlensing in Q2237+0305 and sections 4 and 5 describe the method by which limits can be placed on the mass function through consideration of microlensing due to both a transverse velocity and a stellar velocity dispersion.

2 MICROLENSING AND THE STELLAR MASS FUNCTION

Stellar mass functions have traditionally been measured through the combination of an observed luminosity function and an empirical mass-luminosity relationship. However, because of the difficulties inherent in the observations of faint stars, such determinations become uncertain as the hydrogen burning limit ($\sim 0.08 M_{\odot}$) is approached and crossed. In contrast to this approach, microlensing uses the mass of a lens to magnify the observed flux of a background source through gravitational deflection of the light bundle. The statistics obtained are therefore free of any bias introduced by the hydrogen burning limit, and so microlensing is a powerful tool for determining the contribution to the mass function of low mass stars as well as dark compact objects.

Gravitational microlensing is observed in two very different regimes. Paczynski (1986a) suggested that surveying millions of stars in the Magellanic Clouds for microlensing induced flux variation could be a way of detecting solar mass compact objects in the halo of our own galaxy. Several groups have undertaken such searches (eg. Alcock et al. 1997a; Renault et al. 1998). In a similar vein, Paczynski (1991) and Griest et al. (1991) suggested that microlensing experiments towards the galactic bulge could be used to probe the masses of stars along the line-of-sight in the galactic disc. Microlensing searches towards the bulge have since found a higher rate of microlensing events than are found towards the LMC (eg. Alcock et al. 1997b; Udalski et al. 1994). In a very different microlensing regime, the observed

flux of a back-ground quasar can be altered by gravitational lensing from stars or halo objects in a foreground galaxy. Q2237+0305 is an example of a quasar that lies very close to the galactic line-of-sight. In such cases multiple imaging occurs, allowing microlensed variation to be easily separated from intrinsic fluctuations as these will be observed in all images.

Theoretically the treatments of microlensing in the galactic and cosmological regimes are very different. While there are only a few sources (quasar images) in the cosmological case rather than the millions available in galactic microlensing searches, the optical depth (or equivalently the probability of lensing) is $\sim 10^6$ greater. The transverse velocity is a critical parameter for the determination of the size of a mass or masses responsible for a microlensing event, regardless of the microlensing scenario. Unfortunately it is unknown in both cases. In calculations of galactic microlensing these velocities are inferred from an assumed velocity distribution. However in the cosmological case the transverse velocities of the lensing objects are not independent. Rather, they are equal except for the contribution of the individual stellar proper motions. Moreover, an event in the cosmological case is not dependent on the size of a single mass, but results from the gravitational contribution of a large ensemble of many hundreds of masses. Microlensed, multiply-imaged quasars are an excellent probe of the mass function of compact objects along the quasar image line-of-sight because they interact with a large number of microlenses.

Several authors have placed limits on the masses of microlenses responsible for cosmological microlensing. Schmidt & Wambsganss (1998) use the lack of observed variation in Q0957+561 to place a lower limit on the mass of microlenses in the halo of the lensing galaxy. They rule out halo objects with masses $\ll 10^{-2} M_{\odot}$. However their determination is dependent on the source size, and the fraction of smooth matter employed in their calculations. A transverse velocity of $v_t = 600 \text{ km sec}^{-1}$ is assumed. The uncertainty in this assumed value is the most serious problem in analyses such as this because the value of mass obtained is $\propto v_t^2$. Lewis & Irwin (1996) compared the monitoring data of Q2237+0305 with simulations using a structure function to analyse variability. They too assume a transverse velocity of $v_t = 600 \text{ km sec}^{-1}$ and conclude that the mean mass of objects in Q2237+0305 is $0.1 M_{\odot} < \langle m \rangle < 10 M_{\odot}$. However this determination is again proportional to the square of the unknown transverse velocity.

While they do not measure precisely the same quantity, the above results are supportive of those of the MACHO experiment (eg Alcock et al. 1997a,b). From microlensing towards the LMC by the Galactic halo, Alcock et al. (1997a) conclude that the average MACHO masses are $0.08 - 0.93 M_{\odot}$. The quoted range includes both statistical uncertainties as well as systematic effects introduced by the assumption of halo model. In addition, they find evidence for an excess of events over those predicted from stellar lensing alone. Alcock et al. (1997b) find that the range of time-scales towards the galactic bulge are consistent with microlens masses of $0.1 M_{\odot} < \langle m \rangle < 10 M_{\odot}$. Table 1 summarises the results described.

Table 1. A collection of results from microlensing of the average mass of compact objects in the galactic halo and Bulge.

Milky Way halo (Alcock et al. 1997a)	Results for mean masses of dark halo objects toward LMC. The ranges include statistical (1σ) as well as systematic uncertainties due to choice of halo model.	$\langle m \rangle = 0.13^{+0.08}_{-0.05} M_{\odot}$ $-0.55^{+0.38}_{-0.21} M_{\odot}$
Milky Way bulge (Alcock et al. 1997b)	Microlensing event time-scales are consistent with a mean mass of compact objects and stars in the Milky Way bulge.	$0.1 M_{\odot} < m < 1.0 M_{\odot}$
0957+561 halo (Schmidtt & Wambsganss 1998)	The limit has 99% and 95% significance levels for assumed source sizes of $4 \times 10^{14} cm$ and $4 \times 10^{15} cm$, and scales as the square of the assumed transverse velocity v_t .	$\langle m \rangle > 0.001 \left(\frac{v_t}{600} \right)^2$
2237+0305 bulge and halo (Lewis & Irwin 1996)	The microlensing rate of current light curves is consistent with a mean mass of stars and compact objects. The value scales as the square of the assumed transverse velocity v_t .	$0.1 M_{\odot} < \langle m \rangle \left(\frac{v_t}{600} \right)^2 < 10 M_{\odot}$
2237+0305 bulge and halo This paper.	The proper motions of microlenses provide a minimum micro- lensing rate. The limits given for the mean mass have a 99% significance level, and depend on the bulge dynamics assumed.	$\langle m \rangle = 0.010^{+0.005}_{-0.005} M_{\odot}$ $-0.29^{+0.18}_{-0.18} M_{\odot}$

Table 2. Values of the total optical depth and the magnitude of the shear at the position of each of the 4 images of Q2237+0305. The quoted values are those of Schmidt, Webster & Lewis (1998). κ_* and κ_c are the optical depths in stars and in smoothly distributed matter respectively.

Image	$\kappa = \kappa_* + \kappa_c$	$ \gamma $
A	0.36	0.40
B	0.36	0.40
C	0.69	0.71
D	0.59	0.61

3 THE MICROLENSING MODELS

3.1 Microlensing models for Q2237+0305

Throughout the paper, standard notation for gravitational lensing is used. The Einstein radius of a $1 M_{\odot}$ star in the source plane is denoted by η_0 . The normalised shear is denoted by γ , and the convergence or optical depth by κ . The model for gravitational microlensing consists of a very large sheet of point masses that simulates the section of galaxy along the image line-of-sight, together with a shear term that includes the perturbing effect of the mass distribution of the lensing galaxy as a whole. The normalised lens equation for a field of point masses with an applied shear in terms of these quantities is

$$\vec{y} = \begin{pmatrix} 1 - \kappa_c - \gamma & 0 \\ 0 & 1 - \kappa_c + \gamma \end{pmatrix} \vec{x} + \sum_{j=0}^{N_*} m^j \frac{(\vec{x}^j - \vec{x})}{|\vec{x}^j - \vec{x}|^2} \quad (1)$$

Here \vec{x} and \vec{y} are the normalised image and source positions respectively, and the \vec{x}^j and m^j are the normalised positions and masses of the point masses. κ_c is the optical depth in smoothly distributed matter. To construct a microlensed light-curve Eqn 1 is solved for the macroimage magnification at many points along a predefined source trajectory through the inversion technique of Lewis et al. (1993) and Witt (1993). The region of the lens plane in which im-

age solutions need to be found to ensure that 99% of the total macro-image flux is recovered from a source point was described by Katz, Balbus & Paczynski (1986). In the presence of an applied shear this region is elliptical in shape. The union of the areas of the lens plane that correspond to the flux collection area of each point on the source line is known as the shooting region. The method of determining the dimensions of the shooting region is described in Lewis & Irwin (1995), and Wyithe & Webster (1999). The radius of the disc of point masses is chosen to be 1.2 times that required to cover this shooting region.

For the microlensing models of Q2237+0305 presented in the current work we assume the macro-parameters for the lensing galaxy calculated by Schmidt, Webster & Lewis (1998). These values are shown in table 2. Two models are considered for the distribution of microlenses, one with no continuously distributed matter, and one where smooth matter contributes 50% of the surface mass density. Both the microlensing rate due to a transverse velocity (Witt, Kayser & Refsdal 1993; Lewis & Irwin 1996; Wyithe, Webster & Turner 1999b), as well as the corresponding rate due to proper motions (Wyithe, Webster & Turner 1999a) are not functions of the detail of the microlens mass distribution, but depend only on the mean microlens mass. The mean of the microlens mass function can therefore be determined independently from any assumption that is made about its form. On the other hand, information on the form of the mass function is unobtainable through consideration of the microlensing rate. We therefore limit our attention to models in which all the point masses have an identical mass.

Each of our models was computed for a source track of length $10\eta_0$. We set the minimum number of stars to be used in our models at 500. Two orientations were chosen for the transverse velocity with respect to the galaxy, with the source trajectory being parallel to the A–B or C–D axes. At each orientation, 100 simulations were made for each of the 4 images of Q2237+0305 in combination with each of the model mass distributions. The two orientations bracket the range of possibilities, and because the images are positioned

Table 3. Values for the number of stars in the microlensing models (left column $\gamma > 0$; right column $\gamma < 0$), the average model magnifications and the theoretical values for comparison.

0% smooth matter			
Image	No. Stars	$\langle \mu \rangle$	$\langle \mu_{th} \rangle$
A/B	763	500	3.97 ± 0.28
C	1022	500	2.39 ± 0.11
D	2887	1301	4.79 ± 0.14

50% smooth matter			
Image	No. Stars	$\langle \mu \rangle$	$\langle \mu_{th} \rangle$
A/B	500	500	4.01 ± 0.19
C	500	500	2.44 ± 0.09
D	1080	500	4.84 ± 0.20

approximately orthogonally with respect to the galactic centre correspond to shear values of $\gamma_A, \gamma_B < 0, \gamma_C, \gamma_D > 0$ and $\gamma_A, \gamma_B < 0, \gamma_C, \gamma_D > 0$ respectively. Table 3 shows the number of stars used for each of these models along with the mean magnification $\langle \mu \rangle$, and the theoretical magnification $\langle \mu_{th} \rangle$ for comparison. The average magnification was found from the combination of the two sets of models, and the error calculated from the standard deviation of values computed from a subset of 6 simulations (3 per model orientation). Figure 1 shows the magnification distributions for each image in each model. Simulations having $\gamma < 0$ and $\gamma > 0$ are represented by light and dark lines respectively. This figure demonstrates that the magnification distribution is independent of the source direction as required.

For our analysis we assume that microlensing is produced through the combination of a galactic transverse velocity with each of two classes of proper motion for individual stars with respect to the galaxy, an isotropic velocity dispersion and a circular stream motion. Moreover, we assume that the magnitudes of the dispersion and of the stream motions are the same at the position for each of the four images. For the line-of-sight velocity dispersion of the stars in the galactic bulge we take the theoretical value of $\sigma_* \sim 165 \text{ km sec}^{-1}$. This is lower than the value observed by Foltz et al. (1992) and so any lower limits we place on the mass will be more conservative.

3.2 The effective transverse velocity

We define the effective transverse velocity as the transverse velocity that produces a microlensing rate from a static field model equal to that of the observed light-curve. The effective transverse velocity therefore describes the microlensing rate due to the combination of the effects of a galactic transverse velocity and random proper motion of microlenses.

The procedure for obtaining limits on the effective transverse velocity is discussed in Wyithe, Webster & Turner (1999b). In essence, many simulations are made which have a sampling rate and period that are identical to the published monitoring data (Irwin et al. 1989, Corrigan et al. 1991, Østensen et al. 1996). Observational errors are also simu-

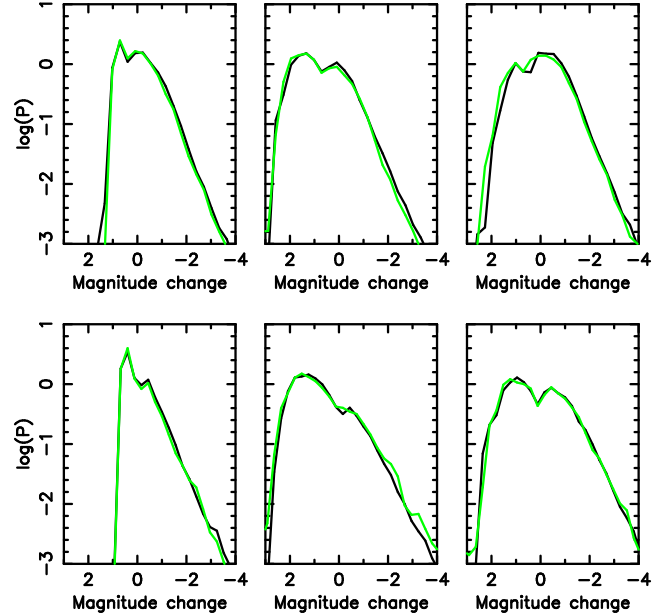


Figure 1. The magnification distributions for images A/B (left), C (centre) and D (right). The top and bottom rows show the distributions for models that have no smooth matter component, and a 50% smooth matter component respectively. The light and dark lines represent distributions that are sampled parallel to and at right angles to the shear respectively.

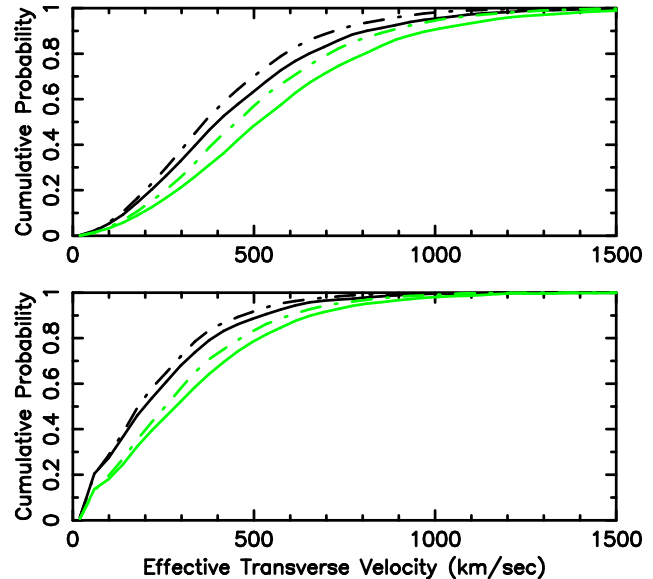


Figure 2. Plots of the upper limit of the measured velocity in Q2237+0305 vs. Monte Carlo confidence (P). The solid and dotted lines correspond to the models with trajectory directions that are aligned with the C-D and A-B image axes respectively. The dark and light lines represent results from models containing 0% and 50% continuously distributed matter. The upper and lower plots correspond to the cases where the photometric error was assumed to be $\sigma_{SE}=0.01$ mag in images A/B and $\sigma_{SE}=0.02$ in images C/D, and $\sigma_{LE}=0.02$ mag in images A/B and $\sigma_{LE}=0.04$ in images C/D.

lated by applying a random Gaussian fluctuation to each point on the sampled light curve.

The simulations used two different estimates of the error in the photometric magnitudes. In the first case a small error was assumed (SE). For images A and B, $\sigma_{SE}=0.01$ mag, and for images C and D $\sigma_{SE}=0.02$ mag. In the second case, a larger error was assumed (LE). For images A and B, $\sigma_{LE}=0.02$ mag and for images C and D $\sigma_{LE}=0.04$ mag. The observational error in Irwin et al. (1989) was 0.02 mag. We note that the adoption of a larger error leads to a smaller bound on the measured upper limit of effective transverse velocity, and subsequently a larger lower bound on the mean mass. In addition, the simulations assume a point source. This follows the results of Wyithe et al. (1999b) where it is shown that the value of effective transverse velocity measured with a model is not a sensitive function of the source size (in the range of interest) assumed. The insensitivity arises from the fact that the measurement is derived predominantly from points that are not part of a HME. The effective transverse velocity for a model of Q2237+0305 is computed using a cumulative histogram of derivatives that is calculated from the 6 difference light-curves (A-B, A-C, A-D, B-C, B-D, C-D). Through computation of the difference light-curves, intrinsic flux variation, as well as the systematic component of the observational uncertainty are removed from the data.

For the current work 5000 sampled simulations were produced at each transverse velocity from the 100 $10\eta_0$ simulations for each model. A time averaged histogram was then computed from each set of simulations. Wyithe, Webster & Turner (1999b) describes a procedure by which the fraction of sampled simulations P that agree less (in terms of the KS difference) with the time averaged histogram than the monitoring data can be computed. P is a measure of the statistical confidence that the effective galactic transverse velocity (V_{gal}) is lower than the assumed value (V_{eff}) for a given microlensing model. This procedure is followed for a series of assumed effective transverse velocities and produces correct upper limits for V_{gal} . However the algorithm uses the magnitude of the KS difference to determine the goodness-of-fit of a given transverse velocity to the simulated microlensing rate. Therefore, at transverse velocities near the most likely value it cannot provide information on the relative microlensing rate of sampled simulations since the shapes of their histograms differ from that of the average histogram. The curve $P(V_{gal} < V_{eff})$ obtained is discontinuous at the most likely transverse velocity. Therefore while $P(V_{gal} < V_{eff})$ converges to the cumulative probability in the upper and lower limits of effective transverse velocity, it does not represent the cumulative probability for all V_{eff} .

To produce a cumulative probability distribution for the effective transverse velocity we have introduced a new method. The ensemble of 5000 sampled simulations as well as the average of these are computed at a series of assumed transverse velocities (V_{eff}). At each effective transverse velocity (V_{eff}), and for each of the sampled simulations, the effective transverse velocity (v_{eff}) is found that minimises the KS difference between the corresponding average histogram and the derivative histogram of the sampled simulation. Through this procedure we calculate the likelihood for v_{eff} ,

$$p_v(v_{eff}|V_{eff}). \quad (2)$$

Similarly the effective transverse velocity (v_{obs}) that best describes the observed microlensing rate can be found. We use Bayes' theorem to calculate the posterior probability that the effective galactic transverse velocity is less than an assumed value V_{eff} :

$$P_v(V_{gal} < V_{eff}|v_{obs}) = \int_0^{V_{eff}} p_v(v_{obs}|V'_{eff}) dV'_{eff}. \quad (3)$$

This expression assumes the flat prior probability $p_v(V_{eff}) \propto dV_{eff}$. We repeated our calculation for the logarithmic prior probability that V_{eff} is equally likely to lie within a given decade ($p_v(V_{eff}) \propto \frac{dV_{eff}}{V_{eff}}$), and found no change in our results. We therefore conclude that our estimate of probability is dominated by the microlensing observations rather than our assumed prior for V_{eff} .

$P(v_{gal} < V_{eff}|v_{obs})$ is plotted in figure 2 for the models discussed in this paper. In these plots the solid and dot-dashed lines correspond to source trajectories along the C-D image axis and A-B image axis, and the dark and light lines correspond to models with 0% and 50% smoothly distributed matter. The upper and lower plots correspond to the cases where the photometric error was assumed to be $\sigma_{SE}=0.01$ mag in images A/B and $\sigma_{SE}=0.02$ in images C/D, and $\sigma_{LE}=0.02$ mag in images A/B and $\sigma_{LE}=0.04$ in images C/D.

3.3 The contribution to microlensing of stellar proper motions

We define the equivalent transverse velocity as the transverse velocity that in combination with a static microlensing model produces a microlensing rate closest to the rate produced in the same model with the transverse velocity replaced by a random velocity dispersion. The microlensing rates are considered equivalent at the transverse velocity that produces a cumulative histogram of light-curve derivatives closest (has the minimum possible KS difference) to the corresponding proper motion histogram.

The formalism required for the computation of the cumulative distribution of derivatives resulting from proper motion of stars was developed in Wyithe, Webster & Turner (1999a). The upper panel of Table 4 shows the values of equivalent transverse velocity computed from the difference light-curves for models of Q2237+0305 (the quoted error describes the range of values obtained over three separate sets of simulations) of a Gaussian 1-d velocity dispersion of $\sigma_* = 165 \text{ km sec}^{-1}$. The microlensing model consisted of $1M_\odot$ stars. The two cases shown are for a trajectory that is parallel to the shear in images A and B ($\gamma_A, \gamma_B > 0$), and for one that is parallel to the shear in images C and D ($\gamma_C, \gamma_D > 0$). In all cases the effective transverse velocity is larger than the 1-d velocity dispersion.

4 PLACING LIMITS ON THE MASS USING EFFECTIVE TRANSVERSE VELOCITY

In this section we describe a method for the determination of the lower limit of the average compact object mass through

Table 4. Table showing the equivalent transverse velocities and the 99%, 95% and 90% lower limits for the mean microlens mass as well as the most likely value. Values for the mass limits are shown corresponding to the cases where the error was $\sigma_{SE} = 0.01$ mags in images A/B, $\sigma_{SE} = 0.02$ mags in images C/D, and where the error was $\sigma_{LE} = 0.02$ mags in images A/B, $\sigma_{LE} = 0.04$ mags in images C/D (in parentheses). Values are shown that correspond to an isotropic velocity dispersion of $\sigma* = 165 \text{ km sec}^{-1}$ (top table), a circular stream velocity of $v_{\text{stream}} = 233 \text{ km sec}^{-1}$ (bottom table).

$\sigma* = 165 \text{ km sec}^{-1}$							
Trajectory Orientation	Smooth Matter	Equiv. Vel. (km sec^{-1})	Bayesian prior	$m_{\text{low}}(99\%)$ (M_{\odot})	$m_{\text{low}}(95\%)$ (M_{\odot})	$m_{\text{low}}(90\%)$ (M_{\odot})	mode (M_{\odot})
Shear: $\gamma_A, \gamma_B > 0, \gamma_C, \gamma_D < 0$	0%	280 ± 15	log	0.050 (0.111)	0.111 (0.277)	0.176 (0.484)	0.139 (0.288)
	50%	199 ± 12	log	0.019 (0.039)	0.042 (0.095)	0.066 (0.161)	0.054 (0.087)
Shear: $\gamma_A, \gamma_B < 0, \gamma_C, \gamma_D > 0$	0%	270 ± 10	log	0.053 (0.111)	0.111 (0.270)	0.173 (0.463)	0.139 (0.281)
	50%	181 ± 4	log	0.018 (0.036)	0.039 (0.084)	0.061 (0.143)	0.042 (0.087)
Shear: $\gamma_A, \gamma_B > 0, \gamma_C, \gamma_D < 0$	0%	280 ± 15	flat	0.098 (0.230)	0.270 (0.739)	0.505 (1.496)	0.222 (0.450)
	50%	199 ± 12	flat	0.042 (0.090)	0.121 (0.301)	0.240 (0.643)	0.069 (0.139)
Shear: $\gamma_A, \gamma_B < 0, \gamma_C, \gamma_D > 0$	0%	270 ± 10	flat	0.107 (0.244)	0.293 (0.792)	0.553 (1.638)	0.222 (0.450)
	50%	181 ± 4	flat	0.044 (0.093)	0.135 (0.330)	0.278 (0.729)	0.069 (0.239)

$v_{\text{stream}} = 233 \text{ km sec}^{-1}$							
Trajectory Orientation	Smooth Matter	Equiv. Vel. (km sec^{-1})	Bayesian prior	$m_{\text{low}}(99\%)$ (M_{\odot})	$m_{\text{low}}(95\%)$ (M_{\odot})	$m_{\text{low}}(90\%)$ (M_{\odot})	mode (M_{\odot})
Shear: $\gamma_A, \gamma_B > 0, \gamma_C, \gamma_D < 0$	0%	129 ± 7	log	0.010 (0.023)	0.024 (0.061)	0.039 (0.113)	0.027 (0.043)
	50%	99 ± 5	log	0.006 (0.011)	0.013 (0.030)	0.022 (0.056)	0.013 (0.021)
Shear: $\gamma_A, \gamma_B < 0, \gamma_C, \gamma_D > 0$	0%	120 ± 2	log	(0.011 (0.023))	0.025 (0.064)	0.042 (0.120)	0.021 (0.043)
	50%	85 ± 3	log	0.005 (0.009)	0.011 (0.024)	0.018 (0.044)	0.010 (0.021)
Shear: $\gamma_A, \gamma_B > 0, \gamma_C, \gamma_D < 0$	0%	129 ± 7	flat	0.028 (0.071)	0.105 (0.319)	0.251 (0.823)	0.034 (0.069)
	50%	99 ± 5	flat	0.014 (0.031)	0.053 (0.144)	0.136 (0.395)	0.017 (0.027)
Shear: $\gamma_A, \gamma_B < 0, \gamma_C, \gamma_D > 0$	0%	120 ± 2	flat	0.027 (0.069)	0.108 (0.33)	0.273 (0.897)	0.034 (0.068)
	50%	85 ± 3	flat	0.014 (0.031)	0.060 (0.159)	0.162 (0.454)	0.017 (0.027)

consideration of the effective transverse velocity as a variable. The microlensing rate has a minimum possible value determined from the size of the stellar velocity dispersion. This is quantified by noting that the effective transverse velocity must be greater than the equivalent transverse velocity.

There is a simple scaling that relates models of the same optical depth but consisting of model stars with a different mass. The dimensionless Einstein radius of a point mass is \sqrt{m} . Therefore, if all masses in the model are reduced by a factor a , then all physical distances (in both the source and lens planes) between dimensionless coordinates are reduced by a factor \sqrt{a} . In the case of a model containing stars with static positions, this results in an increase by a factor of $1/\sqrt{a}$ in the gradient of the light-curve at all points. Similarly, the rate of change of the magnification at a static source point due to stellar proper motions increases by a factor $1/\sqrt{a}$. The minimum rate of microlensing due to proper motions that should be observed is therefore larger for a smaller mean microlens mass. Models do not describe the data if this rate is significantly higher than that observed. The ratio of equivalent transverse velocity to veloc-

ity dispersion is independent of the mean microlens mass. However the gradient of the light-curve scales as $1/\sqrt{a}$, and so the measurement of effective transverse velocity that is made within the context of a given model through comparison with a data set is proportional to \sqrt{a} . This allows limits to be placed on the value of a and therefore the stellar mass from the observed microlensing rate.

5 THE MASS OF COMPACT OBJECTS IN Q2237+0305

5.1 The effect of random proper motions

For a model containing only $1M_{\odot}$ stars, in the case where $\gamma_A, \gamma_B > 0$ and the simulated errors are assumed to be $\sigma_{SE} = 0.01$ and $\sigma_{SE} = 0.02$ mags in images A/B and C/D respectively, the transverse velocity at which 99% of the simulations were more consistent with the time averaged mean than the data was 1346 km sec^{-1} . Therefore, for a model with dimensionless stellar masses of m , the measured upper limit of effective transverse velocity is $V_{\text{upper}}(99\%) = 1346 \times \sqrt{m} \text{ km sec}^{-1}$. In the absence of a

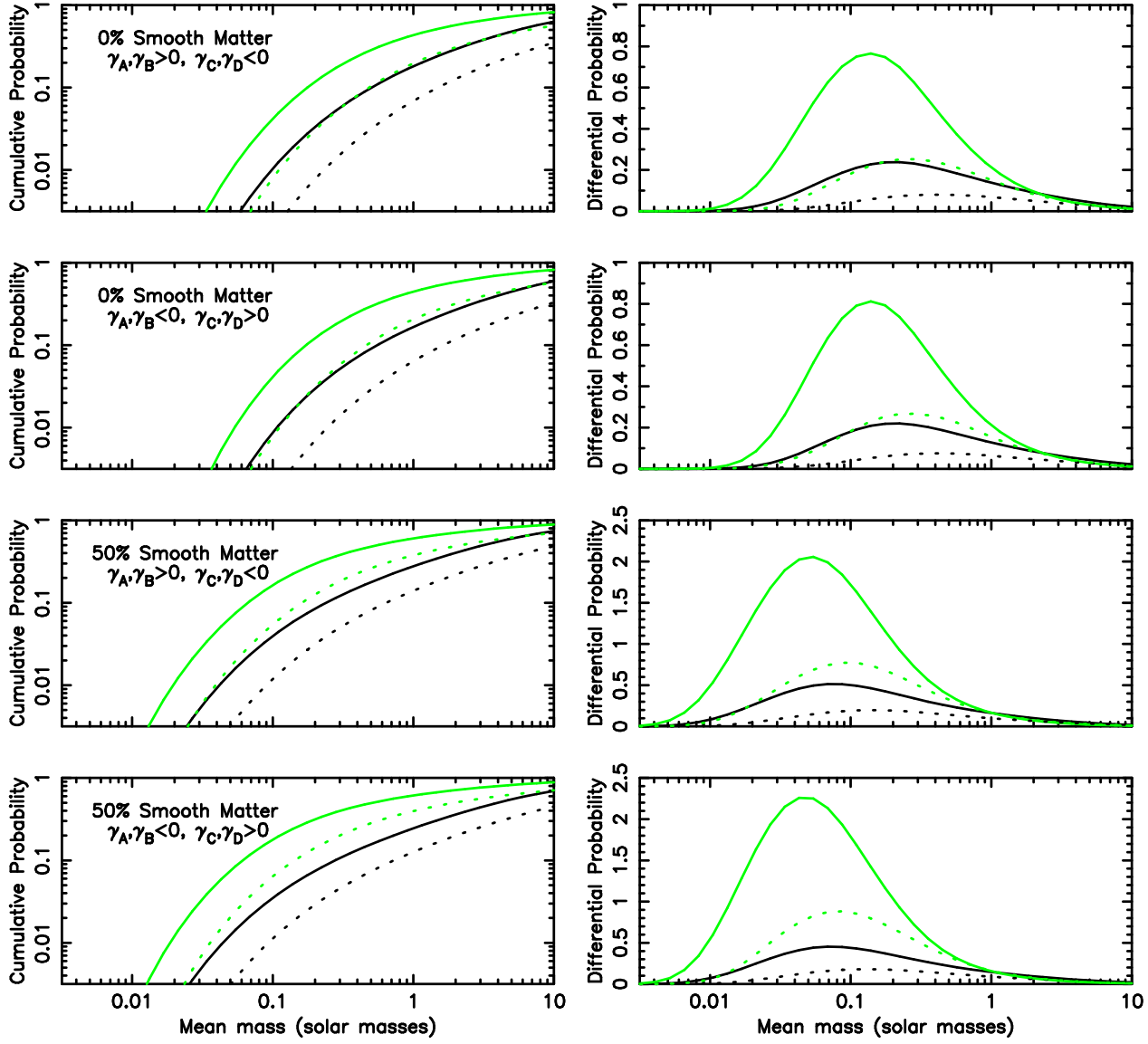


Figure 3. Left: The cumulative distributions, and Right: The differential distributions for the mean microlens mass. The solid and dotted curves represent the resulting functions when the photometric error was assumed to be $\sigma_{SE}=0.01$ mag in images A/B and $\sigma_{SE}=0.02$ in images C/D, and $\sigma_{LE}=0.02$ mag in images A/B and $\sigma_{LE}=0.04$ in images C/D. The light and dark lines correspond to the assumptions of logarithmic and flat priors for transverse velocity referred to in the text.

galactic transverse velocity, there is still a level of microlensing that is described by the equivalent transverse velocity in table 4. This equivalent transverse velocity ($V_{equiv}(DISP)$) represents the minimum level of microlensing that must be observed under the assumption of a given model. Therefore in cases where the measured upper limit drops below this value, the model is unable to explain the observations. Thus prospective models of the bulge may be ruled out on this basis. The value of m at which $V_{upper}(99\%)$ drops below $V_{equiv}(DISP)$ is $m_{low}(99\%)$:

$$m_{low}(99\%) = \left(\frac{V_{equiv}(DISP)}{V_{upper}(99\%)} \right)^2 \sim 0.04. \quad (4)$$

The minimum mass of stars in this model is therefore $\sim 0.04M_{\odot}$. This calculation assumes a value of the one dimensional velocity dispersion of 165 km sec^{-1} . However we

note that all lower limits obtained in this section are proportional to the square of this value. The procedure also assumes that the measured effective transverse velocity is independent of the assumed source size. Wyithe, Webster & Turner (1999a) show that this is approximately true for source sizes smaller than $\approx 4 \times 10^{16} \sqrt{m} \text{ cm}$, and Wambsganss, Paczynski & Schneider (1990) find that a source smaller than $\sim 2 \times 10^{15} \sqrt{\langle m \rangle} / 225 \text{ cm}$ is required to typically reproduce the observed HME amplitude.

The curves shown in figure 2 represent the cumulative probability $P(V_{gal} < V_{eff} \sqrt{m})$ that the effective transverse velocity V_{gal} is less than $V_{eff} \sqrt{m}$. It follows that the cumulative probability of the mean microlens mass being less than the value

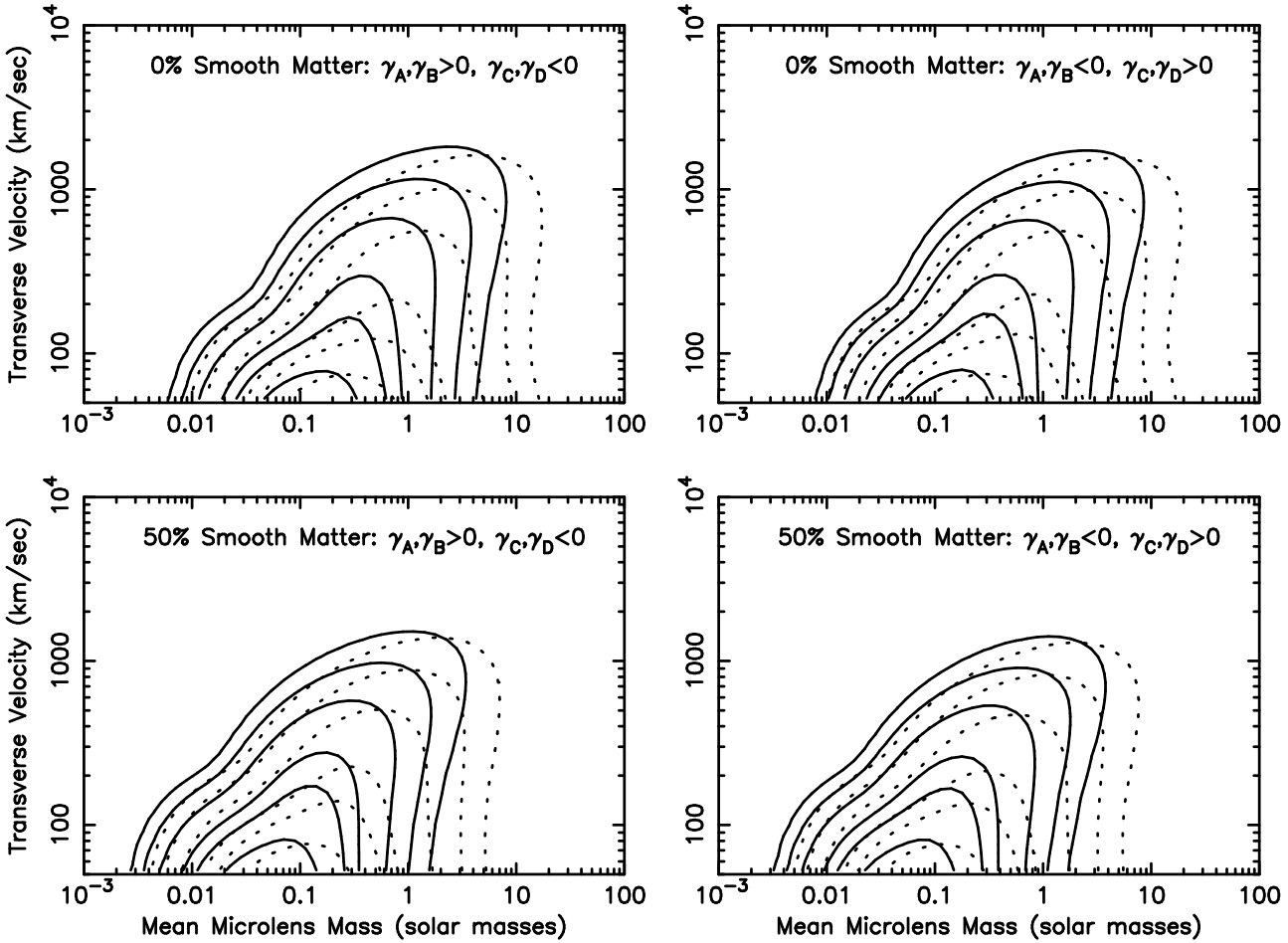


Figure 4. Contours of percentage peak height of the function $p(v_{tran}, \langle m \rangle)$. The contours shown are the 0.1%, 1.0%, 3.6%, 14%, 26% and 61% levels. The solid and dotted curves represent the resulting functions when the photometric error was assumed to be $\sigma_{SE}=0.01$ mag in images A/B and $\sigma_{SE}=0.02$ in images C/D, and $\sigma_{LE}=0.02$ mag in images A/B and $\sigma_{LE}=0.04$ in images C/D.

$$M = \left(\frac{V_{equiv}(DISP)}{V_{eff}} \right)^2 \quad (5)$$

is

$$U(\langle m \rangle < M | V_{equiv}) = 1 - P(V_{gal} < V_{eff} \sqrt{M}). \quad (6)$$

The above calculation assumes that $V_{tran} = 0$. However V_{equiv} is a function of V_{tran} , determined according to the relationships described in Wyithe, Webster & Turner (1999b). While the method outlined determines a minimum mass through noting that there is a maximum possible microlensing rate that is consistent with the observed light curves which must be at least as large as the rate produced by proper motions in the absence of a transverse velocity, there is no corresponding argument to supply an upper limit to the microlens mass. This is because while there is a minimum microlensing rate that is consistent with the observations, microlenses of arbitrarily high mass can produce the required rate in combination with a correspondingly large transverse velocity. Since the galactic transverse velocity is not necessarily zero, U and p_m must be determined at a series of transverse velocities and combined with prior probabilities for V_{tran} to obtain estimates for the probability of the mean microlens mass. We have assumed the

flat and logarithmic priors employed in the calculation of $P(V_{gal} < V_{eff})$ (with a maximum galactic transverse velocity of 2000 km sec^{-1}):

$$U(\langle m \rangle < M) = \int U(\langle m \rangle < M | V_{tran}) p_v(V_{tran}) dV_{tran} \quad (7)$$

By taking the derivative $\frac{dU}{d\langle m \rangle}$ the probability density $p_m(\langle m \rangle)$ for the mean microlens mass can be obtained. Note that this distribution does not represent the mass function. $p_m(\langle m \rangle | V_{tran})$ is extremely sensitive to the level of photometric error assumed at large $\langle m \rangle$. In addition, $p_m(\langle m \rangle)$ at large $\langle m \rangle$ is a function of the prior assumed due to the degeneracy between $\langle m \rangle$ and V_{tran} . Therefore $p_m(\langle m \rangle)$ does not place useful upper limits on the mean microlens mass.

Figure 3 shows the functions $U(\langle m \rangle < M)$ (left hand columns) and $p_m(\langle m \rangle)$ (right hand columns) for the 0% smooth matter and 50% smooth matter models for each of the two directions considered. The solid and dotted curves represent the resulting functions when the photometric error was assumed to be $\sigma_{SE}=0.01$ mag in images A/B and $\sigma_{SE}=0.02$ in images C/D, and $\sigma_{LE}=0.02$ mag in images A/B and $\sigma_{LE}=0.04$ in images C/D. The light and dark lines refer to the logarithmic and flat priors for transverse velocity. Re-

sults for $m_{low}(99\%)$, $m_{low}(95\%)$, $m_{low}(95\%)$ and the mode of the distribution are shown in the top panel of Table 4. In each column, values are shown that correspond to the two assumptions for the simulated error referred to above. $m_{low}(99\%)$ is $> 0.02M_{\odot}$ in all models considered. The mode of the distribution ranges between $0.04M_{\odot}$ and $0.45M_{\odot}$. It is interesting to note that these models produce distribution modes that are similar to the mean of a Salpeter distribution with a lower cutoff at the hydrogen burning limit. We also note that the distribution is highly asymmetric, with the mode being of the same order as the lower limit.

In contrast to the calculation of $P(V_{gal} < V_{eff} \sqrt{\langle m \rangle})$ the prior assumed makes a significant difference to the results obtained. In particular, if high transverse velocities are assumed to be relatively likely, the computed probability of the microlenses having a large mass becomes higher. This dependence on the prior assumed illustrates the limitation of the light curve data for breaking the degeneracy between velocity and microlens mass in the high mass-velocity regime.

The two assumptions for photometric error produce a variation in the measurements of transverse velocity, and therefore of the mean microlens mass. As discussed Wyithe, Webster & Turner (1999b) the adoption of a larger error yields a lower estimate of the transverse velocity because the error introduces independent variation between images into the flat parts of the light-curve. This in turn means that a larger estimate is made for the mean microlens mass. The effect is readily apparent in figure 3 as well as from table 4.

Our results are dependent on the fraction of smooth matter that is assumed in the model. This is due to the combination of a determination of a larger effective transverse velocity and a smaller relative contribution to microlensing of the stellar proper motions, which results in a smaller minimum of the observed microlensing rate. This must be the case since in the situation of a galaxy that is composed entirely of continuously distributed matter no microlensing will be observed. The plots in figure 3 demonstrate the level of dependence on smooth matter component.

To explore the co-dependence of the determined mean microlens mass and galactic transverse velocity we have computed the two dimensional distribution

$$p_m(\langle m \rangle, V_{tran}) = p_m(\langle m \rangle | V_{tran}) p_m(V_{tran} | \langle m \rangle). \quad (8)$$

Figure 4 shows contour plots of this distribution for the assumed source orientations, smooth matter fraction and photometric errors. All possible combinations of the two values of each parameter are included, so that eight models are shown. The contours are at 0.1, 1.0, 3.6, 14, 26, 61 percent of the peak height, and so the extrema of the inner 4 contours represent 4σ , 3σ , 2σ , and 1σ limits on the single variables. The most important benefit of combining the distributions of V_{tran} and $\langle m \rangle$ is that upper limits can be placed on the mean microlens mass and galactic transverse velocity. The limits on $\langle m \rangle$ and V_{tran} are subject to both random and systematic uncertainties. Assuming that the chosen values for these parameters bracket the likely models, upper and lower limits for $\langle m \rangle$, and an upper limit for V_{tran} can be found by using the most extreme values of the contour limits. This yields the 95 per cent result that $0.01M_{\odot} \lesssim \langle m \rangle \lesssim 1M_{\odot}$, and a galactic transverse velocity less than $\sim 300 \text{ km sec}^{-1}$ (95%). The upper limit is lower than that obtained by Lewis & Irwin (1996), although sufficiently high that it does not

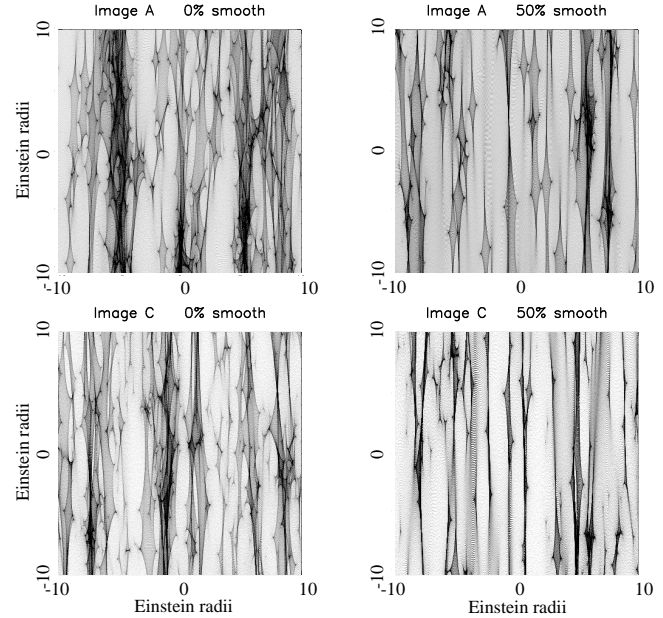


Figure 5. The magnification maps for images A (top) and C (bottom), in the cases of 0% smooth matter (left) and 50% smooth matter (right). The point masses each had a mass of $1M_{\odot}$.

conflict with any popular models of galactic halos or bulges. The elongation of the outer contours with a power law slope of $\frac{1}{2}$ illustrates the degeneracy between microlens mass and transverse velocity at large mass.

5.2 The effect of trajectory direction

The measured effective transverse velocity is dependent on trajectory direction, with a larger measurement resulting from cases where the source trajectory is perpendicular to the shear in images C and D ($\gamma_C, \gamma_D < 0$). This larger measurement indicates that the caustic network is more elongated, or stretched in these images, creating a larger difference between the rate of microlensing for sources moving with and against the shear. The variation with orientation in the measurements of effective transverse velocity is slightly larger when the model contains a component of smooth matter.

Figure 5 shows the magnification maps for images A and C in the cases of 0% and 50% continuously distributed matter. The figure shows that upon the introduction of smooth matter the overall density of caustics is reduced, resulting in a larger measurement of transverse velocity (see figure 2). In addition, the caustic networks in both images become significantly more stretched, resulting in many almost linear fold caustics. This linearity indicates that a source could travel a significant distance in the direction of caustic clustering and be subject to very little microlensed flux variation. The reason for this behaviour can be seen from the lens equation transformation of Paczynski (1986b). He showed that a model containing an optical depth in continuously distributed matter of κ_c plus an optical depth in stars κ_* with an applied shear of γ is mathematically equivalent to a model containing only point masses, but with $\kappa = \kappa_* \times |1 - \kappa_c|$ and $\gamma = \gamma / |1 - \kappa_c|$ (following appropriate

scaling of source and image lengths). The optical depth in the scaled model is lowered while the shear is raised. Moreover, the fraction by which these parameters change is larger at higher optical depths. In Q2237+0305 the images with larger optical depths also posses larger shear values, hence the rather extreme magnification pattern in the smooth matter case of image C.

A similar argument applies to the determination of the equivalent transverse velocity of a stellar velocity dispersion. The rate of microlensing due to stellar proper motions at a series of fixed source points is independent of the direction in which those points are sampled, regardless of the contributing fraction of smoothly distributed matter. However microlensing that results from a transverse velocity has a rate that varies more with direction in images C and D. The equivalent transverse velocity is therefore a function of direction. The effect is more pronounced in models that include a smoothly distributed mass component. In addition, the rate of microlensing that results from a velocity dispersion is lower if the model contains a component of smooth matter.

Thus there are two separate effects. Firstly there is an increase of the measured effective transverse velocity in the case where the source trajectory is aligned with the image C-D axis. This effect is magnified by the inclusion of a component of smooth matter. In addition, the equivalent transverse velocity of the stellar proper motions is also increased under the same circumstances. Interestingly, for our measurement of the lower mass limit, these effects tend to have a cancelling effect. Our measurement of a lower mass limit is therefore reasonably insensitive to the source trajectory direction that is assumed.

5.3 The effect of stream motions

Section 5.1 assumed that microlensing results from the combination of stellar proper motions and a galactic transverse velocity. However the bulge dynamics may be dominated by rotational motion resulting in stream motions of the starfield. For an isothermal sphere model of the bulge, the rotational velocity is $\sqrt{2}\sigma_* = 233 \text{ km sec}^{-1}$. Kundic, Witt & Chang (1993) obtained the expression for the caustic velocity that results from a stream motion. For a stream motion of $\vec{v}_{\text{stream}} = (v_{\text{stream}}, 0)$, the caustic velocity is

$$v_{\text{caust}} = (1 - \gamma - \kappa_c) \times v_{\text{stream}}. \quad (9)$$

If the rotational motion is assumed to be circular then the stream motions are perpendicular to the image-galactic centre axis, and therefore parallel to the shear vector at each image. We choose the stream motions to be in the x_1 direction, the shear is therefore positive at the position of each image ($\gamma > 0$). Six difference light-curves can be constructed from the image light-curves, and an equivalent transverse velocity defined for the stream motions at each image through a method that is identical to the one described for the stellar proper motions in section 5.1. Equivalent transverse velocities were calculated for the two transverse directions discussed previously, for a circular stream motion of $v_{\text{stream}} = 233 \text{ km sec}^{-1}$ ($V_{\text{equiv}}(\text{STREAM})$). These values are presented in Table 4. When combined with the equivalent velocities presented in section 5.1 for an isotropic velocity dispersion, these equivalent transverse

velocities represent the contribution to the microlensing rate of the extreme cases for stellar motions in the galactic bulge.

Table 4 shows results for $m_{\text{low}}(99\%)$, $m_{\text{low}}(95\%)$, $m_{\text{low}}(90\%)$ and the mode for all models considered. $m_{\text{low}}(99\%)$ is $> 0.005M_{\odot}$ in all models where the bulge contains stream motions only. The equivalent transverse velocities presented in table 4 show that an orbital stream motion produces a much lower microlensing rate than a transverse velocity of equal magnitude regardless of its direction. The reason for this behaviour can be seen from Eqn 9. For a stream motion that is moving parallel to the shear vector the caustic velocity decreases with increasing shear. In addition, the caustic velocity and hence microlensing rate are also decreased when there is a component of smooth matter. In this case the effect is especially strong since including smooth matter also increases the effective shear. The lower microlensing rate translates to an equivalent transverse velocity that is much smaller than the one obtained from a stellar velocity dispersion. This in turn means a lower estimate of $m_{\text{low}}(P)$. In the case we have presented, $v_{\text{stream}} = \sqrt{2}\sigma_*$, the mass limit obtained is only ~ 0.2 times that where the proper motions are assumed to be isotropic.

The last row of Table 1 summarises the range of values obtained by this study for the mean microlens mass. These compare favourably with the results of related studies, none of which find that Jupiter mass compact objects are the dominant component of mass in the bulges and or halos of the spiral galaxies studied.

6 CONCLUSION

Calculations of the transverse velocity from published monitoring data of Q2237+0305, as well as complimentary characterisations of caustic clustering from previous papers show that the caustic networks produced by populations of microlenses have a structure that is independent of the mass spectrum. However the scale length is proportional to the square root of the mean mass. Previous determinations of average mass from microlensing data have therefore been proportional to the square of the unknown transverse velocity. However a minimum rate of microlensing will be produced by the proper motions of microlenses in the bulge of the lensing galaxy. We have used limits on the transverse velocity obtained from published monitoring data for Q2237+0305 in combination with calculations of the microlensing effect of isotropic stellar proper motions in the bulge to calculate functions representing the probability for the mean microlens mass. We find that the most likely value for the mean microlens mass is $0.04\text{--}0.45M_{\odot}$. The lower limits on the mean microlens mass responsible for the observed microlensing are $\langle m \rangle > 0.02\text{--}0.24M_{\odot}$ (99% level). A similar calculation assuming an orbital stream motion of stars in the bulge rather than a velocity dispersion produces a most likely value of $0.01\text{--}0.05M_{\odot}$ and a lower limit of $\langle m \rangle > 0.005\text{--}0.071M_{\odot}$ (99% level).

Through joint consideration of the probability for mean microlens mass and transverse velocity under the assumption of an isotropic velocity dispersion we obtain a mass between $0.01M_{\odot}$ and $1.0M_{\odot}$ (95%), and a transverse velocity less than 300 km sec^{-1} (95%).

While these values depend on the correctness of the

published macrolensing parameters, as well as on the fraction of smoothly distributed matter assumed, they do not depend on any other unknowns present in the problem including the source size, source profile, transverse velocity and direction of the source trajectory. A significant contribution of Jupiter mass compact objects to the mass distribution of the bulge is therefore unambiguously ruled out whether the microlenses move predominantly in orbital or random motions. However if the microlens proper motions are distributed according to an isotropic velocity dispersion then the lower limit obtained is of the same order as the hydrogen burning limit.

REFERENCES

- Corrigan et.al, 1991, Astron. J., 102, 34
 Foltz, C. B., Hewitt, P. C., Webster, R. L., Lewis, G. F., 1992,
 Ap. J., 386, L43
 Griest K. et al. 1991, Ap. J., 372, L79
 Irwin, M. J., Webster, R. L., Hewitt, P. C., Corrigan, R. T., Je-
 drzejewski, R. I., 1989, Astron. J., 98, 1989
 Katz, N., Balbus, S., Paczynski, B., 1886, Ap. J., 306, 2
 Kent, S. M., Falco, E. E., 1988, Astron. J., 96, 1570
 Lewis, G. F., Irwin, M. J., 1995, MNRAS 276, 103
 Lewis, G. F., Irwin, M. J., 1996, MNRAS 283, 225
 Østensen, R. et al. 1996, Astron. Astrophys., 309, 59
 Paczynski, B., 1986a, Ap. J., 304, 1
 Paczynski, B., 1986b, Ap. J., 301, 503
 Paczynski, B., 1991, Ap. J., 371, L63
 Renault, C., et al., 1998, Astron. Astrophys., 329, 522
 Schmidt, R. W., Webster, R. L., Lewis, G. F. 1998, MNRAS, 295,
 488
 Schmidt, R. W., Wambsganss, J., 1998, Astron. Astrophys., 335,
 379
 Schneider, D. P., Turner, E. L., Gunn, J. E., Hewitt, J. N.,
 Schmidt, M., Lawrence, C. R., 1988, Astron. J., 95, 1619
 Udalski, A., et al., 1994, Ap. J., 435, L113
 Wambsganss, J., Paczynski, B., Schneider, P., 1990, Ap. J., 358,
 L33
 Wyithe, J. S. B., Webster, R. L., 1999, MNRAS accepted
 Wyithe, J. S. B., Webster, R. L., Turner, E. L., 1999a, MNRAS
 submitted
 Wyithe, J. S. B., Webster, R. L., Turner, E. L., 1999b, MNRAS
 accepted
 Witt, H. J., 1993, Ap. J., 403, 530
 Witt, H. J., Kayser, R., & Refsdal, S. 1993, Astron. Astro-
 phys., 268, 501